Mathematical Modelling for Wave Drag Optimization and Design of High-Speed Aircrafts

Can Citak, Serkan Ozgen and Gerhard Wilhelm Weber

Abstract Supersonic flight has been the subject of last half century. Both civil and defence projects have been running to design an aircraft to fly faster than speed of sound. Developing technology and increasing experience of design leads to faster, fuel efficient, hence, ecological, long-ranged aircrafts. These vehicles make people live easy by shortening travel time, perform missions with powerful defence aircrafts and helping explore space. Aerodynamic design is the main argument of the high speed aircrafts improvement. Having less supersonic drag force, which is greater than the double of subsonic case for conventional aircraft, is the ultimate goal of the aircraft designers at supersonic speed. In this chapter, an aerodynamic characteristics of the entire configuration is optimized in order to reach this aim. Moreover, solver algorithm is validated with computational fluid dynamics simulations for different geometries at various speeds. The objective of this study is to develop a program which optimizes wave drag coefficient of high speed aircrafts by numerical methods.

Keywords Supersonic flight · Wave drag · Optimization · Area rule

1 Wave Drag Definition

Designing an aircraft with the ability of flying faster than the speed of sound was the purpose of most aircraft designers in the past decades in order to reduce travel time and research space. Both aims require ultimate design configurations for definite missions. Unlike the subsonic design, the supersonic region has struggles to deal with in order to reach this aim. The major part of this problem is about the huge drag

C. Citak (✉) · S. Ozgen · G.W. Weber
METU, Ankara, Turkey
e-mail: ccitak@ae.metu.edu.tr

S. Ozgen
e-mail: sozgen@ae.metu.edu.tr

G.W. Weber
e-mail: gweber@metu.edu.tr

A.A. Pinto and D. Zilberman (eds.), *Modeling, Dynamics, Optimization and Bioeconomics II*, Springer Proceedings in Mathematics & Statistics 195,
DOI 10.1007/978-3-319-55236-1_7

force occurring when compared to subsonic speed. Thus, aircraft designers aware of these drawbacks were in a need of making modifications to their design. For example, re-entry of an spacecraft which is directly related to drag force must be considered as one of the critical issue of the overall design process.

Wave drag can be described as the major part of the force resisting aircraft motion at supersonic speed. It depends on the velocity of the aircraft, wing area, air density and drag coefficient which are related to complete configuration of the aircraft. The main purpose in an aircraft design is generally to reduce drag to minimum level. On the other hand, drag force is beneficial for some extreme cases, such as the utilization of parachute for short distance landing. Drag is mainly classified as drag due to lift and zero lift drag. The work represented in this chapter mainly concentrates on the wave drag (zero lift). Temperature, pressure, aircraft velocity and the shape of the configuration affects the magnitude of the wave drag. When supersonic free stream reaches an obstacle, shock wave occurs which increases the density and pressure of the flow. In other words, the free stream Mach number, which must be greater than 1 for shock wave to occur, decreases below Mach 1 after the normal shock formation [5]. The shock wave leads to increase in entropy and reduction in total pressure. If the shock wave is inevitable, the efficiency of the shock formation can be increased in order to reduce the total increase of entropy. A wing with sweep angle and fuselage shaping can be used for this purpose. This study aims at minimizing wave drag coefficient without changing the aerodynamic characteristics of the lifting surfaces. Thus, the area distribution and the volume of the fuselage is modified to reach the minimum value of the objective function.

As seen in Fig. 1 [14], the supersonic drag of an aircraft rises 3–4 times of the subsonic case so that the drag optimization of the supersonic aircraft is the main criterion of the aerodynamic design process. The aircraft shape might be optimized despite the fact that the composition of it seems suitable for the residential of sub-

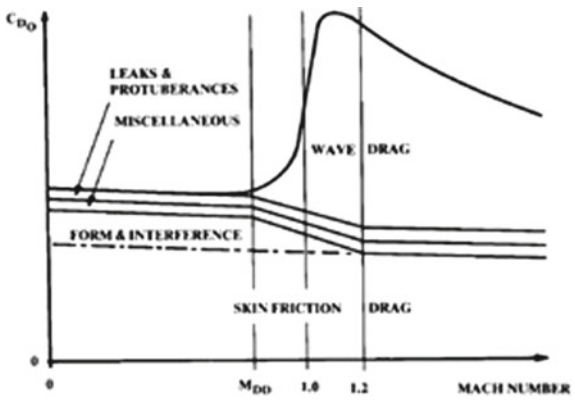

Fig. 1 Drag variation with mach number [14]

components. Nevertheless, the optimal shape of aircraft are not being implemented to the base design due to the manufacturing and sub-component constraints which give rise to additional drag. Small changes in supersonic drag could be critical. To illustrate this, on the *Concorde*, [16] it can be stated that one count drag increase ($\triangle C_d = 0.0001$) requires two passengers, out of the 90–100 passenger capacity, be taken off the North Atlantic run [16]. Additional drag components at supersonic speed are wave drag due to lift and wave drag due to volume. Wave drag due to lift vanishes as Mach number goes to one or aspect ratio goes to zero. Consequently, wave drag due to volume is investigated in this research. The behavior of the volume wave drag at various Mach numbers and different geometries are observed.

2 Far-Field Theory

Total momentum change in streamwise direction of control volume is equal to the drag of the aircraft. Inlet region is the only undisturbed flow passing through the aircraft geometry which becomes two dimensional because of the pressure effects. Thus, the momentum change between inlet and outlet regions (streamwise momentum change) is the sum of all the drag contributors. In addition, subsonic flow becomes parallel at outlet if the control volume is large enough. On the other hand, mass flows in and out from the side of the cylinder at supersonic speed due to shock and expansion wave formations [15, 17] (Fig. 2).

Total change in momentum as a result of mass flow in and out is defined as wave drag. Moreover, since the shock formation varies with the angle of attack, wave drag can change with the angle of attack as well. Therefore, wave drag is formed with wave drag due to volume and wave drag due to lift which produces the effects of wave drag variation due to lift. The drag equation is given in Eq. (1) as

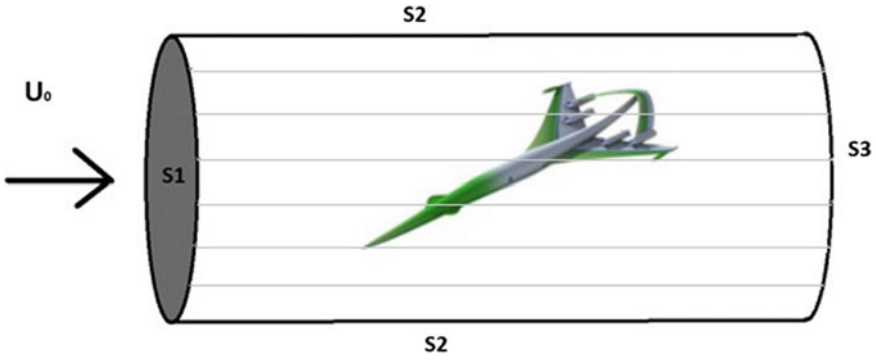

Fig. 2 Control volume representation [19]

$$\iint_{S_3=S_1} (p - p_\infty)\, dS_3 - \rho_\infty U_\infty^2 \iint_{S_3=S_1} \phi_x\, (1 + \phi_x)\, dS_3 - \rho_\infty U_\infty^2 \iint_{S_2} \phi_x \phi_r\, dS_2 + \sum D_{misc}\ . \quad (1)$$

Miscellaneous drag consists of excrescence and base drags. If the control volume is located far enough, flow becomes two dimensional, the stream wise perturbation velocity is zero. Thus the second integral in the general drag formula becomes zero as

$$\rho_\infty U_\infty^2 \iint_{S_3=S_1} \phi_x\, (1 + \phi_x)\, dS_3 = 0\ , \quad (2)$$

and the gauge pressure is formulated as

$$p - p_\infty\ = -\frac{1}{2}\rho_\infty U_\infty^2\, (\phi_x^2 + \phi_z^2)\ . \quad (3)$$

Since the viscosity effects are neglected, the total inviscid drag equation can be written as shown below:

$$D = -\rho_\infty U_\infty^2 \iint_{S_2} \phi_x \phi_r\, dS_2 + \frac{1}{2}\rho_\infty U_\infty^2 \iint_{S_2} (\phi_y^2 + \phi_z^2)\, dS_3\ . \quad (4)$$

Wave drag can be calculated directly from mass flow change at side surface of the control volume. Perturbation velocities in the first integral give the velocity change in side direction. As these are multiplied with the density and the square of free stream velocity, the total wave drag could be obtained. The wave drag formula is given in Eq. (5):

$$D_w = -\rho_\infty U_\infty^2 \iint_{S_2} \phi_x \phi_r\, dS_2\ . \quad (5)$$

Farfield linear theory has positive and negative characteristics. First, it is simply used for calculations. In addition, singularities can be overcome without sophisticated numerical methods; i.e., pressure calculations at leading edge. As shown in Eq. (4), induced drag can be separated from wave drag by using far field linear theory which provides pure wave drag calculation. Thus, it is useful for area rule optimization with respect to wave drag. Since the volume of the aircraft is the only contributor to drag formula, aircraft geometry can be directly related to the wave drag. Hence, aircraft area distribution can be modified in order to minimize wave drag. On the contrary, the theory does not reflect physics of the flow completely. Therefore, aircraft design could be validated with other methods to ensure behavior of the flow over aircraft surface [2].

2.1 Formula Transformation

Conventional form of the wave drag is given as

$$D_w = -\frac{1}{2\pi} \int_0^1 \int_0^1 S''(x)S''(y)\ log|x-y|\ dxdy\ . \tag{6}$$

Two problems arise in the calculation of the formula given above. Firstly, singularity occurs where the longitudinal locations of the aircraft become identical. Secondly, numerical precision strongly depends on the differentiation method used and the degree of accuracy. Thus, a sensitivity analysis is effective for calculation of wave drag force. Two conditions must be satisfied for the method used to obtain wave drag:

1. The first derivative of the area distribution is continuous along longitudinal direction of aircraft.
2. The first derivatives of the area distribution at nose and rear regions are equal to zero:

$$S'(0) = S'(L) = 0\ , \tag{7}$$

where L represents the length of aircraft. When the conditions explained above are satisfied, the first derivative of the area distribution can be transformed to the Fourier sine series as,

$$x = \frac{1}{2}\ (1 - \cos\theta)\ , \tag{8}$$

where θ varies between 0 and π:

$$\theta = \cos^{-1}(1 - 2x)\ . \tag{9}$$

Subsequently, we refer to Eqs. (8) and (9) implicitly. Then the first derivative distribution is given by

$$S'(x) = \sum_{r=1}^{\infty} a_r\ \sin r\theta\ , \qquad 0 \leq\ x \leq 1\ , \tag{10}$$

where the coefficient is written as

$$a_r\ = \sum_{r=1}^{\infty} \frac{2}{\pi} \int_0^{\pi} S'(x) r\theta d\theta\ . \tag{11}$$

The area distribution of the aircraft is obtained by integrating the Eq. (10) as

$$S(x) = \sum_{r=1}^{\infty} a_r \int_0^{\pi} \sin r\theta dx \ . \tag{12}$$

Equation (9) is integrated and substituted into Eq. (11) by using the derivative of Eq. (8):

$$dx = -\frac{1}{2} \sin\theta \ d\theta \ , \tag{13}$$

hence,

$$S(x) = \frac{1}{2} \sum_{r=1}^{\infty} a_r \int_0^{\pi} \sin r\theta \sin\theta d\theta,$$

$$= a + \frac{1}{4} a_1 \ (\theta - \frac{1}{2} \ \sin 2\theta) + \frac{1}{4} \sum_{r=2}^{\infty} a_r [\frac{\sin(r-1)\theta}{r-1} \ - \frac{\sin(r+1)\theta}{r+1} \ ],$$

$$= a + \frac{1}{4} a_1 \ \theta + \frac{1}{4} \sum_{r=1}^{\infty} (a_r - a_r - 1) \sin r\theta \ . \tag{14}$$

By using Eq. (13), the second derivative of the area distribution is obtained and inserted into Eq. (6) as

$$D_w = \frac{1}{2} \int_0^{\pi} \sum_{r=1}^{\infty} a_s \ \sin s\theta d\theta,$$

$$= \frac{1}{2} \sum_{r=1}^{\infty} \sum_{s=1}^{\infty} r a_r a_s \int_0^{\pi} \sin r\theta \sin s\theta d\theta,$$

$$= \frac{\pi}{4} \sum_{s=1}^{\infty} r a_r^2 \ . \tag{15}$$

Gradient-based optimization method is used in order to obtain the area distribution which has minimum wave drag force. Since the accuracy of the gradient calculation strictly depends on the smoothness of the objective function and constraints.

3 Mathematical Modelling

3.1 Cross-Sectional Area Calculation

Greens theorem is used for the calculation of cross-sectional area [10]. The incremental area dA is defined as

$$dA = dxdy \ . \tag{16}$$

It states that area A of a closed region D can be represented as

$$A = \iint_D dA \ . \tag{17}$$

Furthermore, M and L are functions having continuous partial derivatives defined by the boundaries of D:

$$\frac{\partial M}{\partial x} - \frac{\partial L}{\partial y} = 1 \ . \tag{18}$$

The area of A is given as

$$A = \oint_C (Ldx + Mdy) \ . \tag{19}$$

The final form of the area formula can be written as

$$A = \frac{1}{2} \oint_C (-ydx + xdy) \ . \tag{20}$$

Area computation for each cross-section is necessary as being inputs to the solver, since the shape of the cross-sections are arbitrary with variable number of points. Equation (19) is used to calculate this area. Figure 3 indicates the arbitrary shaped cross section:

$$S = \frac{1}{2} \sum_{i=1}^{n-1} (y_i x_{i+1} - y_{i+1} x_i) \ . \tag{21}$$

3.2 Fourier Transformation

The Fourier transformation methodology is defined as fitting the data set or any type of the polynomial to sinusoidal function(s). General formulation for the polynomial curve fitting is written as

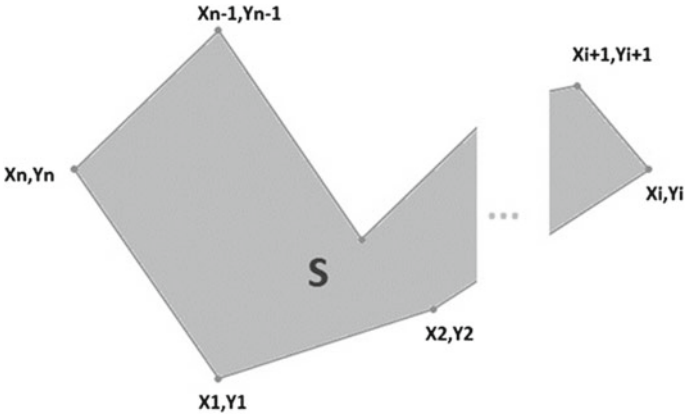

Fig. 3 Arbitrary shaped area

$$y = a_0 + a_1 x + a_1 x^2 + \cdots + a_m x^n \ . \tag{22}$$

The residual is calculated as

$$S_r = \sum_{i=1}^{n} (y_i - a_0 - a_1 x - a_1 x^2 - \cdots - a_m x^n)^2 \ ; \tag{23}$$

this fit of the curve accuracy has to be optimized. Thus, gradients of the residual is zero when the curve fitting represents the data set successfully. The gradients are given by

$$\frac{\partial S_r}{\partial a_0} = -2 \sum_{i=1}^{n} (y_i - a_0 - a_1 x - a_1 x^2 - \cdots - a_m x^n) \ , \tag{24}$$

$$\frac{\partial S_r}{\partial a_1} = -2 \sum_{i=1}^{n} x_i (y_i - a_0 - a_1 x - a_1 x^2 - \cdots - a_m x^n) \ , \tag{25}$$

$$\frac{\partial S_r}{\partial a_2} = -2 \sum_{i=1}^{n} x_i^2 (y_i - a_0 - a_1 x - a_1 x^2 - \cdots - a_m x^n) \ , \tag{26}$$

$$\vdots$$

$$\frac{\partial S_r}{\partial a_n} = -2 \sum_{i=1}^{n} x_i^n (y_i - a_0 - a_1 x - a_1 x^2 - \cdots - a_m x^n) \ . \tag{27}$$

The coefficients are obtained by equating and solving the gradient equations as

$$(n)a_0 + (\sum x_i)a_1 + (\sum x_i^2)a_2 + \cdots + (\sum x_n^m)a_m = \sum y_i \ , \tag{28}$$

$$(\sum x_i)a_0 + (\sum x_i^2)a_1 + (\sum x_i^3)a_2 + \cdots + (\sum x_n^{m+1})a_m = \sum x_i y_i \ , \tag{29}$$

$$(\sum x_i^2)a_0 + (\sum x_i^3)a_1 + (\sum x_i^4)a_2 + \cdots + (\sum x_n^{m+2})a_m = \sum x_i^2 y_i \ , \tag{30}$$

$$\vdots$$

$$(\sum x_i^n)a_0 + (\sum x_i^{n+1})a_1 + (\sum x_i^{n+2})a_2 + \cdots + (\sum x_n^{m+n})a_m = \sum x_i^m y_i \ . \tag{31}$$

The same approach can be used for the Fourier transformation. The polynomial function can be changed into the sinusoidal variables in order to fit the Fourier transformation to data set. Equation (30) represents first order Fourier model. Application of the transformation is presented as follows:

$$y = a_0 + a_1 \cos(\omega t) + b_1 \sin(\omega t) \ . \tag{32}$$

The residual of the model is given as

$$S_r = \sum_{i=1}^{n} (y_i - a_0 + a_1 \cos(\omega t) + b_1 \sin(\omega t))^2 \ , \tag{33}$$

the gradients of the residual S_r are represented by

$$\frac{\partial S_r}{\partial a_0} = -2 \sum_{i=1}^{n} (y_i - A_0 + A_1 \cos(\omega t) + B_1 \sin(\omega t)) \ , \tag{34}$$

$$\frac{\partial S_r}{\partial a_1} = -2 \sum_{i=1}^{n} \cos(\omega t)(y_i - A_0 + A_1 \cos(\omega t) + B_1 \sin(\omega t)) \ , \tag{35}$$

$$\frac{\partial S_r}{\partial a_2} = -2 \sum_{i=1}^{n} \sin(\omega t)(y_i - A_0 + A_1 \cos(\omega t) + B_1 \sin(\omega t)) \ . \tag{36}$$

A necessary condition for success of convex curve fitting operation is that the gradient equations are equal to zero. Then, the unknown coefficients are obtained from solutions of set of equations. In this section, first derivative of the cross-sectional area distribution is transformed into Fourier sine function. The reason of this process is that the first derivative of cross-sectional area distribution must be continuous according to the wave drag calculation methodology. Equation (35) represents the open form of the sine function. In addition, smoothness is one of the most important criteria for minimization procedure. Thus, representation of real cross-sectional area

distribution must be accurate enough [2, 4, 12]. Furthermore, value of error function shown in Eq. (31), does not reduce linearly. Therefore, to keep CPU at a certain level and to obtain valid representation, fourth-order sine functions are chosen;

$$y = a_0 + a_1\cos(x) + b_1\sin(x) + a_2\cos(2x) + b_2\sin(2x) \\ +a_3\cos(3x) + b_3\sin(3x) + a_4\cos(4x) + b_4\sin(4x)\ . \tag{37}$$

The function S_r' gives the difference between discrete response data and the approximated function.

$$S_r' = \sum_{i=1}^{N}(y_i - y)^2\ , \tag{38}$$

we require:

$$\frac{\partial S_r'}{\partial a_0}, \frac{\partial S_r'}{\partial a_1}, \frac{\partial S_r'}{\partial a_2}, \frac{\partial S_r'}{\partial a_3}, \frac{\partial S_r'}{\partial a_4}, \frac{\partial S_r'}{\partial b_1}, \frac{\partial S_r'}{\partial b_2}, \frac{\partial S_r'}{\partial b_3}, \frac{\partial S_r'}{\partial b_4} = 0\ . \tag{39}$$

3.3 Point Update

Updating the points after optimization step is the final operation of the program. Simple methodology is used for this work. Initial cross-sectional area magnitude at ith location S_{init_i} is calculated as explained in the previous section. Then, optimal cross-sectional area magnitude S_{opt_i} is obtained after the optimization process. The ratio R_i is defined by

$$S_{opt_i} = S_{init_i} + \Delta S_i\ , \tag{40}$$

$$R_i = \sqrt{\frac{S_{opt_i}}{S_{init_i}}}\ . \tag{41}$$

With respect to initial X and Y locations, jth order of ith section; $P_{X_{ijinit}}$ and $P_{Y_{ijinit}}$ are updated as follows:

$$Px_{ij_{opt}} = R_i \cdot Px_{ij_{init}}\ , \tag{42}$$

$$Py_{ij_{opt}} = R_i \cdot Py_{ij_{init}}\ . \tag{43}$$

All cross-sections except for the control surfaces are updated as explained above. The idea behind the use of ratio R_i is that the slope of the points belonging to the same cross-section is kept constant. The slopes of $P_{ij_{init}}$ and $P_{ij_{opt}}$ can be written as,

$$C_{ij_{init}} = \frac{Py_{ij_{init}}}{Px_{ij_{init}}}, \quad C_{ij_{opt}} = \frac{Py_{ij_{opt}}}{Px_{ij_{opt}}} \tag{44}$$

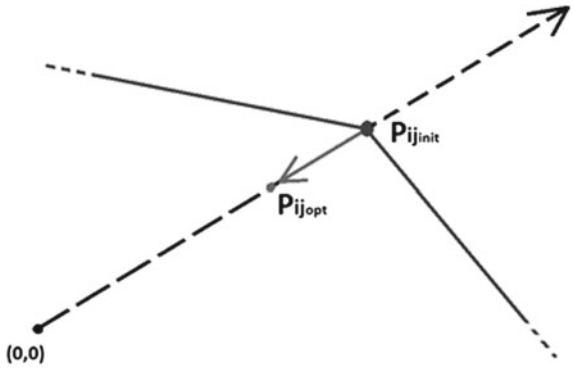

Fig. 4 Point update representation

and

$$C_{ij_{opt}} = C_{ij_{init}} = \frac{Py_{ij_{init}} \cdot R_i}{Px_{ij_{init}} \cdot R_i} \ . \tag{45}$$

To illustrate them, Fig. 4 represents the methodology behind the point update. Assuming that the final cross-sectional area is less than the initial area, then, the slope of the point can be kept constant, and updated with respect to ratio of optimal and initial cross-sectional area. Thus, the shape of the geometry is protected, which means that the initial conceptual design criteria is protected.

Furthermore, some additional steps must be investigated for non-symmetric cases. The center of the cross section must be found. Theoretically, x_c and y_c are the central locations of jth cross-section:

$$x_{c_j} = \frac{1}{n} \sum_{i=1}^{n} x_{init} \ , \tag{46}$$

$$y_{c_j} = \frac{1}{n} \sum_{i=1}^{n} y_{init} \ , \tag{47}$$

the slopes of each point in non-symmetric cross-section are

$$C_{ij_{init}} = \frac{y_{init} - y_{c_j}}{x_{init} - x_{c_j}} \ . \tag{48}$$

Since the slope is kept constant, two unknowns and two equations arise:

$$C_{ij_{opt}} = \frac{y_{opt} - y_{c_j}}{x_{opt} - x_{c_j}} \ , \tag{49}$$

$$\sqrt{(x_{init} - x_{cj})^2 + (y_{init} - y_{cj})^2} \cdot R = \sqrt{(x_{opt} - x_{cj})^2 + (x_{opt} - x_{cj})^2} \ . \tag{50}$$

Coordinates of the optimal form of the cross-sectional area distribution can be obtained by solving Eqs. (47) and (48). This approach provides an analysis of more realistic configurations.

4 Theory of Lagrange Multipliers

The methodology of Lagrange multiplier is employed for the constrained optimization. This part presents the method used for minimization of wave drag coefficient. A general formulation can be represented as

$$\min f(x) \quad \text{subject to} \begin{cases} c_i(x) = 0, & i \in \varepsilon, \\ c_i(x) \geq 0, & i \in I, \end{cases}$$

where the both objective function and constraints are smooth, real-valued functions. $i \in \varepsilon$ are the equality constraints, $i \in I$ are the inequality constraints. There are more than one local solutions for an objective function both for constrained and unconstrained cases. Smoothness of the objective functions and constraints is critical for the global convergence. Furthermore, sharp changes of these functions might mislead the search direction. To avoid that, the functions having sharp edges could characterized which can be represented with collection of smooth functions. For a simple example, Lagrangian function for one equality constraint is shown as

$$L(x, \lambda) = f(x) - \lambda_1 c_1(x) \ , \tag{51}$$

where $f(x)$ is the objective and $c_1(x)$ is the equality constraint function. The optimality condition is given as

$$\nabla_x L(x^*, \lambda_1^*) = 0, \ \text{and} \ \lambda_1^* \geq 0 \ . \tag{52}$$

Despite the fact that equation shown above is necessary for optimal solution, it is not sufficient already. It is also required that the following complementarity condition holds:

$$\lambda_1^* c_1(x^*) = 0. \tag{53}$$

Let us emphasize that, in our project, the objective function will be strictly convex, guaranteeing that our candidate solution will be a real solution. Generally, the Lagrangian function for the constrained optimization problem is defined as,

$$L(x, \lambda) = f(x) - \sum_{i=1}^{n} \lambda_i c_i(x) \ . \tag{54}$$

The active set $i \in A(x) \subseteq I$ at any feasible x is the union of the set with the indices of the active inequality constraints (where $c_i(x) = 0$ is fulfilled) [7]. Next, the linear

independence constraint qualification (*LICQ*) holds since the set of active constraint gradients is linearly independent. Finally, the open form of the first-order necessary conditions is written as

$$\nabla_x L(x^*, \lambda^*) = 0 \,, \tag{55}$$

$$c_i(x^*) = 0 \,, \text{ for all } i \in \varepsilon \,, \tag{56}$$

$$c_i(x^*) \geq 0 \,, \text{ for all } i \in I \,, \tag{57}$$

$$\lambda_i^* \geq 0 \,, \text{ for all } i \in I \,, \tag{58}$$

$$\lambda_i^* c_i(x^*) = 0 \,, \text{ for all } i \in \varepsilon \cup I \,. \tag{59}$$

The multi-constrained (equality) optimization method is subsequently employed for this study. Theory of Lagrange multiplier for related subjects is explained in detail. Considering the case of objective function $f(x, y, z)$ to be minimized with respect to constraints $c_1(x, y, z)$ and $c_2(x, y, z)$. The Lagrangian function is written as

$$L(x, y, z, \lambda_1, \lambda_2) = f(x, y, z) - \lambda_1 c_1(x, y, z) - \lambda_2 c_2(x, y, z) \,, \tag{60}$$

the optimality condition is reached when,

$$\nabla f(x^*, y^*, z^*) = \lambda_1 \nabla c_1(x^*, y^*, z^*) + \lambda_2 \nabla c_2(x^*, y^*, z^*) \,. \tag{61}$$

Open form of the equations are represented as,

$$0 = L_x(x^*, y^*, z^*, \lambda_1, \lambda_2) = f_x(x^*, y^*, z^*) - \lambda_1 c_{1_x}(x^*, y^*, z^*) - \lambda_2 c_{2_x}(x^*, y^*, z^*) \,, \tag{62}$$

$$0 = L_y(x^*, y^*, z^*, \lambda_1, \lambda_2) = f_y(x^*, y^*, z^*) - \lambda_1 c_{1_y}(x^*, y^*, z^*) - \lambda_2 c_{2_y}(x^*, y^*, z^*) \,, \tag{63}$$

$$0 = L_z(x^*, y^*, z^*, \lambda_1, \lambda_2) = f_z(x^*, y^*, z^*) - \lambda_1 c_{1_z}(x^*, y^*, z^*) - \lambda_2 c_{2_z}(x^*, y^*, z^*) \,, \tag{64}$$

$$0 = L_{\lambda_1}(x^*, y^*, z^*, \lambda_1, \lambda_2) = c_1(x^*, y^*, z^*) \,, \tag{65}$$

$$0 = L_{\lambda_2}(x^*, y^*, z^*, \lambda_1, \lambda_2) = c_2(x^*, y^*, z^*) \,, \tag{66}$$

where λ_1 and λ_2 are Lagrange multipliers, "$*$" denotes the optimal condition.

4.1 Optimization Procedure

Since the area distribution is defined two different sine function which are independent, the wave drag formula is transformed into Eq. (65) (a_0 represents the *nose area* which is equal to zero):

$$D = \sum_{n=1}^{\infty} (na_n^2 + nb_n^2) \ . \tag{67}$$

The coefficients a_n and b_n above are the parameters in the Fourier transformation in Eq. (35). The permanent constraint function [9] which defines the total volume of the aircraft is defined as

$$V = \frac{1}{2} \sum_{i=1}^{k-1} (y_{i+1} + y_i) \cdot (x_{i+1} + x_i) \ , \tag{68}$$

where y represents the Fourier transformation of area distribution. The volume function is created by using a simple trapezoid rule [15]. The second constraint function is generated for keeping ith cross sectional area constant [19]. Equation (67) shows the constraint function of area

$$S_i = S_c \ . \tag{69}$$

In open form of Eqs. (66) and (67) are written as

$$C_1 = \frac{1}{8} \sum_{i=1}^{n-1} (a_1\theta + a_2 \sin\theta + 4(a_3 - a_1) \sin 2\theta + (a_4 - a_2) \sin 3\theta + b_1\theta + b_2 \cos\theta \\ +4(b_3 - b_1) \cos 2\theta + (b_4 - b_2) \cos 3\theta) \cdot (x_{i+1} - x_i) - V = 0, \tag{70}$$

$$C_2 = \big(a_1\theta + a_2 \sin\theta + 4(a_3 - a_1) \sin 2\theta + (a_4 - a_2) \sin 3\theta + b_1\theta + b_2 \cos\theta \\ + 4(b_3 - b_1) \cos 2\theta + (b_4 - b_2) \cos 3\theta\big) - S_c = 0. \tag{71}$$

Lagrangian conditions are given by

$$0 = L(a_1, a_2, a_3, a_4, b_1, b_2, b_3, b_4, \lambda_1, \lambda_2)_{a_1} = f_{a_1}(a_1, a_2, a_3, a_4, b_1, b_2, b_3, b_4) - \\ \lambda_1 C_{1_{a_1}}(a_1, a_2, a_3, a_4, b_1, b_2, b_3, b_4) - \lambda_2 C_{2_{a_1}}(a_1, a_2, a_3, a_4, b_1, b_2, b_3, b_4), \tag{72}$$

$$0 = L(a_1, a_2, a_3, a_4, b_1, b_2, b_3, b_4, \lambda_1, \lambda_2)_{a_2} = f_{a_2}(a_1, a_2, a_3, a_4, b_1, b_2, b_3, b_4) - \\ \lambda_1 C_{1_{a_2}}(a_1, a_2, a_3, a_4, b_1, b_2, b_3, b_4) - \lambda_2 C_{2_{a_2}}(a_1, a_2, a_3, a_4, b_1, b_2, b_3, b_4), \tag{73}$$

$$0 = L(a_1, a_2, a_3, a_4, b_1, b_2, b_3, b_4, \lambda_1, \lambda_2)_{a_3} = f_{a_3}(a_1, a_2, a_3, a_4, b_1, b_2, b_3, b_4) - \lambda_1 C_{1_{a_3}}(a_1, a_2, a_3, a_4, b_1, b_2, b_3, b_4) - \lambda_2 C_{2_{a_3}}(a_1, a_2, a_3, a_4, b_1, b_2, b_3, b_4), \quad (74)$$

$$0 = L(a_1, a_2, a_3, a_4, b_1, b_2, b_3, b_4, \lambda_1, \lambda_2)_{a_4} = f_{a_4}(a_1, a_2, a_3, a_4, b_1, b_2, b_3, b_4) - \lambda_1 C_{1_{a_4}}(a_1, a_2, a_3, a_4, b_1, b_2, b_3, b_4) - \lambda_2 C_{2_{a_4}}(a_1, a_2, a_3, a_4, b_1, b_2, b_3, b_4), \quad (75)$$

$$0 = L(a_1, a_2, a_3, a_4, b_1, b_2, b_3, b_4, \lambda_1, \lambda_2)_{b_1} = f_{b_1}(a_1, a_2, a_3, a_4, b_1, b_2, b_3, b_4) - \lambda_1 C_{1_{b_1}}(a_1, a_2, a_3, a_4, b_1, b_2, b_3, b_4) - \lambda_2 C_{2_{b_1}}(a_1, a_2, a_3, a_4, b_1, b_2, b_3, b_4), \quad (76)$$

$$0 = L(a_1, a_2, a_3, a_4, b_1, b_2, b_3, b_4, \lambda_1, \lambda_2)_{b_2} = f_{b_2}(a_1, a_2, a_3, a_4, b_1, b_2, b_3, b_4) - \lambda_1 C_{1_{b_2}}(a_1, a_2, a_3, a_4, b_1, b_2, b_3, b_4) - \lambda_2 C_{2_{b_2}}(a_1, a_2, a_3, a_4, b_1, b_2, b_3, b_4), \quad (77)$$

$$0 = L(a_1, a_2, a_3, a_4, b_1, b_2, b_3, b_4, \lambda_1, \lambda_2)_{b_3} = f_{b_3}(a_1, a_2, a_3, a_4, b_1, b_2, b_3, b_4) - \lambda_1 C_{1_{b_3}}(a_1, a_2, a_3, a_4, b_1, b_2, b_3, b_4) - \lambda_2 C_{2_{b_3}}(a_1, a_2, a_3, a_4, b_1, b_2, b_3, b_4), \quad (78)$$

$$0 = L(a_1, a_2, a_3, a_4, b_1, b_2, b_3, b_4, \lambda_1, \lambda_2)_{b_4} = f_{b_4}(a_1, a_2, a_3, a_4, b_1, b_2, b_3, b_4) - \lambda_1 C_{1_{b_4}}(a_1, a_2, a_3, a_4, b_1, b_2, b_3, b_4) - \lambda_2 C_{2_{b_4}}(a_1, a_2, a_3, a_4, b_1, b_2, b_3, b_4), \quad (79)$$

$$0 = L(a_1, a_2, a_3, a_4, b_1, b_2, b_3, b_4, \lambda_1, \lambda_2)_{\lambda_1} = C_1 , \quad (80)$$

$$0 = L(a_1, a_2, a_3, a_4, b_1, b_2, b_3, b_4, \lambda_1, \lambda_2)_{\lambda_2} = C_2 . \quad (81)$$

In order to reach the optimality conditions, a search direction is utilized to update iterative algorithm. The search direction is written as

$$\nabla f(a_1, a_2, a_3, a_4, b_1, b_2, b_3, b_4, \lambda_1, \lambda_2) = \lambda_1 C_1(a_1, a_2, a_3, a_4, b_1, b_2, b_3, b_4) + \lambda_2 C_2(a_1, a_2, a_3, a_4, b_1, b_2, b_3, b_4) . \quad (82)$$

A convergence criterion is satisfied as soon as $\|\nabla L\|_2 \leq \varepsilon$ at the regarded point, for some given $\varepsilon > 0$.

5 Validation of the Solver with F-16 Aircraft Geometry

The solver used for the calculation of the wave drag force and coefficient is validated with CFD results. The wave drag coefficient of the F-16 aircraft at Mach 2 is obtained for comparison with Rallabhandi's result [13]. Figure 5 represents the mesh of the geometry.

Fig. 5 F-16 mesh

Table 1 Comparison of the results

Mach number	Rallabhandi's result C_{D_w}	Present study C_{D_w}
2.00	0.0357	0.0330

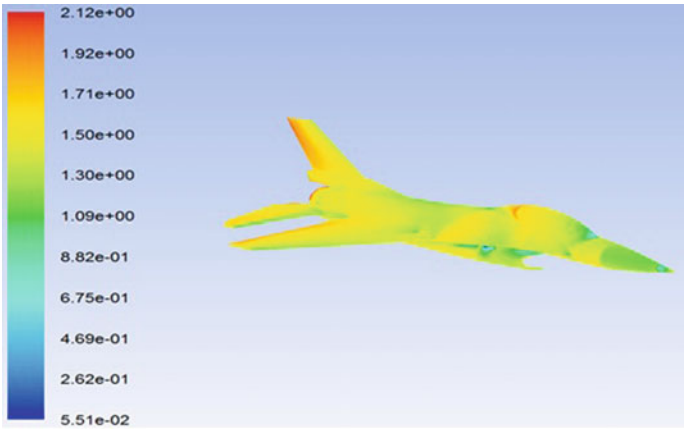

Fig. 6 Mach contours of F-16

Since the Sears-Haack slender body has continuous first derivative, the stability of wave drag computation could be achieved by using sufficient number of cross-sections. On the other hand, the geometry of F-16 aircraft has discontinuities which directly affects the area distribution. Five different size of elements representing the aircraft geometry are employed in order to obtain the mesh-independent solutions. 6.7 millions elements are created for the half aircraft in Fig. 5 [3].

The CFD analysis of F-16 is completed at Mach = 2 for comparison of the results which are shown in Table 4. There, it can be seen that difference between wave drag coefficients of Rallabhandi and of present study is 5.7% (Table 1).

Figure 6 represents the Mach contours of the $F-16$.

6 Results

The optimal forms of the configurations are represented in this section. Nonlifting surfaces are modified during the optimization loop in order not to change the aerodynamic characteristics of the aircraft configurations. In other words, fuselage is reshaped to minimize wave drag coefficient. Mach cuts plays an important role on calculating wave drag force for an arbitrary shaped aircraft. Equation (81) represents the Mach angle which is used for calculating intercepted area distribution without using the *Mach cone approach*. In detail, the aerodynamic characteristics of an aircraft must remain unchanged during optimization. Therefore, lifting and control surfaces and related cross-sections are excluded for the optimization algorithm. Furthermore, the total volume of the aircraft is calculated by summing all parts despite exclusion of lifting and control surfaces. In other words, non-lifting surfaces are modified with respect to the objective function. Second, the intercepted cross-sectional area distribution for various Mach number is obtained by neglecting the small changes due to Mach cone method. It can be stated that non-lifting surfaces of a high-speed aircraft must be as smooth as possible due to avoid the flow separation and shock formation. For this reason, nonlifting surfaces such as fuselage does not have sharp changes which brings out the intercepted area distribution for various Mach numbers could be obtained with *Mach angle methodology* only [6, 8]:

$$\mu = \sin^{-1}\left(\frac{1}{Mach}\right) . \tag{83}$$

Despite the fact that the Mach number seems influential the optimization process, the optimal cross sectional area distribution is independent from the Mach number. Mach number only affects the intercepted area distribution only. Thus, Sears–Haack slender body has the minimum wave drag coefficient for a given volume and length. However, the intercepted area distribution and wave drag coefficient of it change with respect to the Mach number. To have the minimum value of the wave drag force coefficient for an aircraft, the change of first derivative of cross-sectional area distribution of the entire aircraft has to be minimum for a given volume and length. The methodology explained above is commonly used for high subsonic and supersonic aircraft design development. (*Feet and degree are used as length and angle units for all cases*.)

6.1 Conceptual Aircraft Design

Lifting and control surfaces are not modified during optimization in order not to alter aerodynamic characteristics of the aircraft. In addition, theoretical validation is the most important argument. Despite the fact that optimal shape of the conceptual aircraft design is not the best choice for manufacturability, theoretical aspect of the

Table 2 Wing specifications of the conceptual aircraft design

	Wing
Airfoil	NACA 63A304
Chord	2-24
Span	18.55
Sweep	45
Dihedral	0

Table 3 Tail specifications of the conceptual aircraft design

	Tail
Area	103.2
Sweep	45
Dihedral	12.3
Airfoil	4% BICONVEX
Span	0

Table 4 Fuselage specifications of the conceptual aircraft design

	Fuselage
Length	72.75
Volume	45

optimal form is satisfying. Specifications of the conceptual aircraft design are given in Tables 2, 3 and 4.

Figures 7 and 8 represent the initial and the optimal configurations of conceptual aircraft design. As seen in Fig. 8, wing and tail area distribution affect the fuselage shape to obtain the optimal area distribution. Furthermore, theoretical aspects of the optimization method provide the optimal conceptual aircraft configuration despite the fact that applicability to actual design projects requires advanced design methods. To illustrate this, optimal form of the geometry can be utilized by using wing-body concepts for high-speed UAVs.

Fuselage area distribution is modified as seen in Fig. 9. Total volume and length of the aircraft are kept constant during optimization.

6.2 Supersonic Aircraft Geometry with GE F – 414

More practical point of view than the theoretical approach can be obtained by employing supersonic aircraft on use for drag minimization. Since the cross-sectional area of air intakes are subtracted from entire area distribution with respect to linearized theory, Figs. 10, 11 and 12 represent the comparison between the optimal and initial form of the three dimensional supersonic aircraft configuration without air intakes. Tables 5, 6 and 7 represent the specifications of the supersonic aircraft.

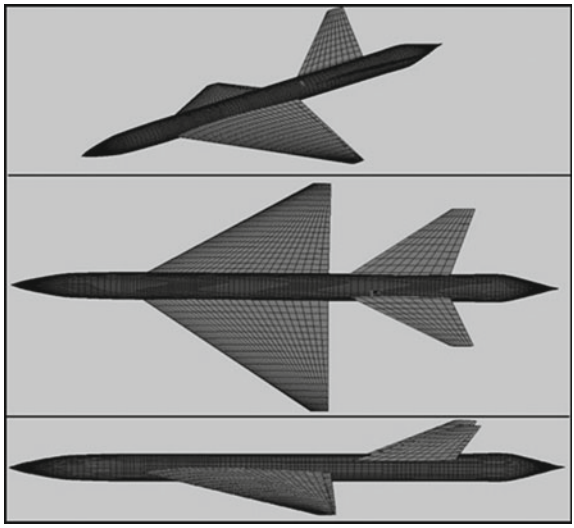

Fig. 7 Initial conceptual aircraft geometry

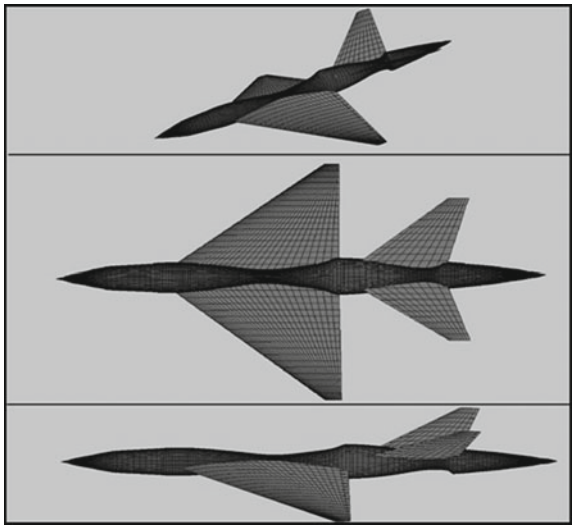

Fig. 8 Optimal conceptual aircraft geometry

The diameter and length of $GE\ F-414$ are 3.96 ft and 15.18 ft [18]. According to these dimensions, minimum cross-sectional area for the engine region is 15.4 ft^2 (minimum cross-sectional area is calculated by multiplying the area of the engine with 1.20). Thus, the locations representing engine location are fixed to this value.

The wave drag coefficient of the supersonic aircraft is reduced from 0.185 to 0.171 with the constraints explained above. Total volume of the aircraft is not kept constant in order to avoid unnecessary increase in nose and canopy region. In detail, magnitude of areas related to engine section are fixed by employing simple calculation which is

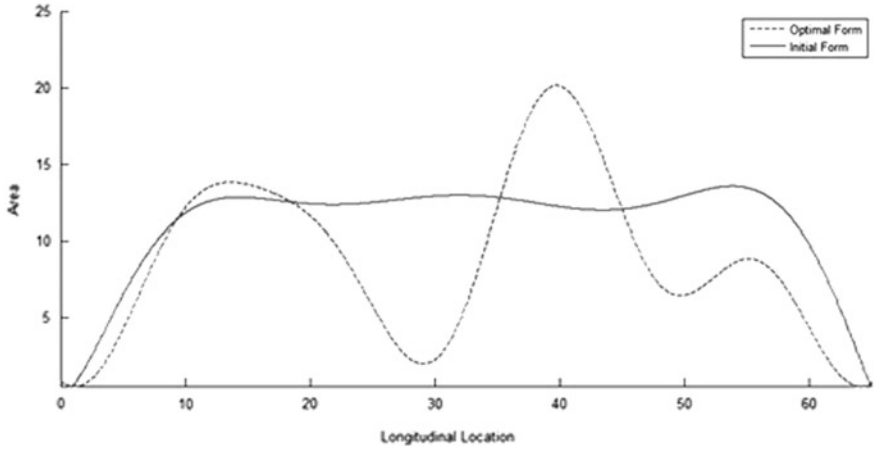

Fig. 9 Comparison of initial and optimal fuselage area distribution

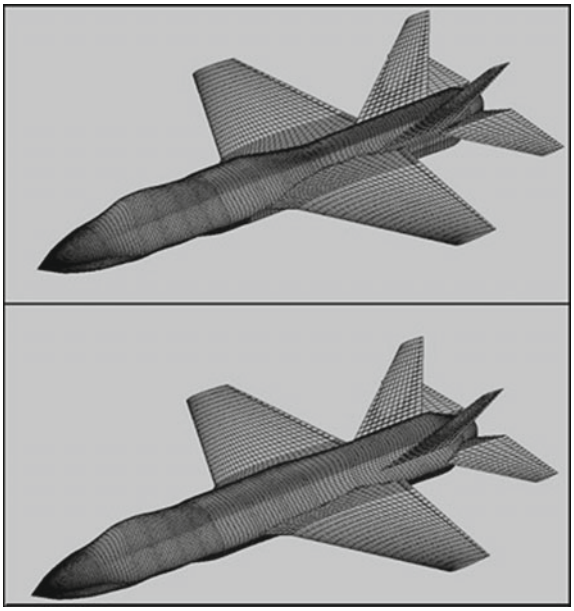

Fig. 10 Initial *(bottom)* and final *(top)* configuration of supersonic aircraft-isometric

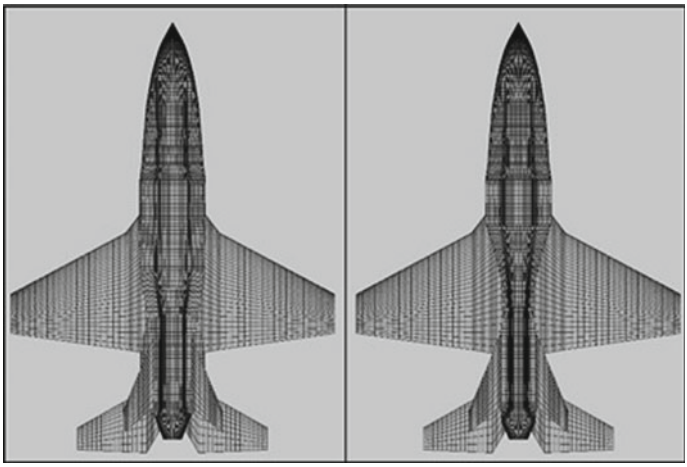

Fig. 11 Initial *(left)* and final *(right)* configuration of supersonic aircraft-top

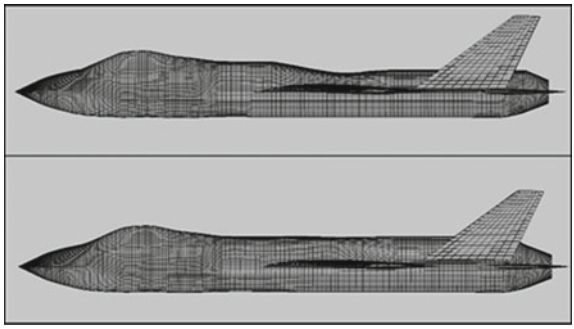

Fig. 12 Initial *(bottom)* and final *(top)* configuration of supersonic aircraft-side

Table 5 Wing specifications of supersonic aircraft

	Section 1	Section 2
Span	5.13	12.59
Tip chord	12.73	4.26
Root chord	20.43	12.73
Sweep	52	28
Dihedral	0	0

less than the initial magnitudes [14]. Theoretically, volume participants at the front region of the aircraft increases to keep volume constant which results in impractical decision. To provide this, constraints of engine section is used for optimization. Finally, Fig. 13 represents the initial and the optimal fuselage area distribution of the supersonic aircraft geometry with $GE\ F-414$. The lower part of the fuselage must have a place for landing gear and other components. Thus, an area reduction is applied for the upper part of the fuselage as seen in Fig. 12.

Table 6 Vertical tail specifications of supersonic aircraft

	Section 1	Section 2
Span	1.77	7.36
Tip chord	8.05	2.30
Root chord	8.05	12.73
Sweep	0	50
Dihedral	0	60

Table 7 Horizontal tail specifications of supersonic aircraft

	Section 1	Section 2
Span	2.84	7.53
Tip chord	6.99	2.37
Root chord	3.76	6.99
Sweep	29.52	29.52
Dihedral	0	60

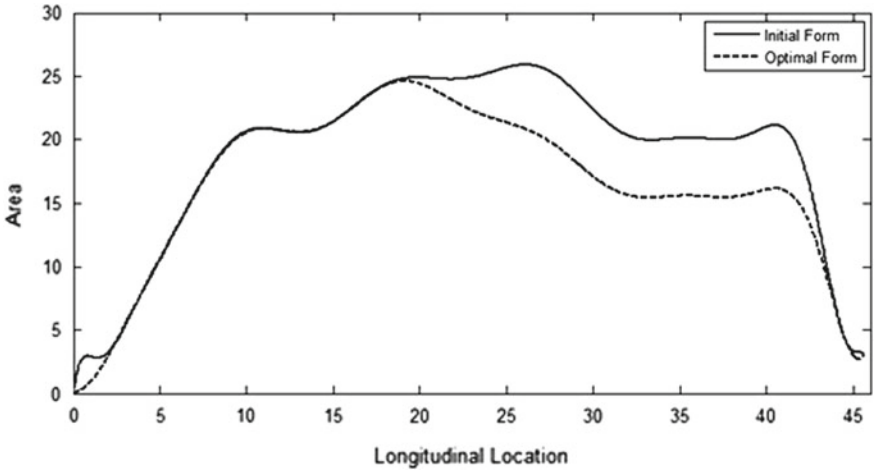

Fig. 13 Comparison of initial and optimal fuselage area distribution (supersonic aircraft configuration with $GE\ F-414$)

7 Conclusion and Discussion

In this chapter, the numerical optimization of the wave drag is performed. At the early stages of research, a literature survey is completed on methods about wave drag calculation, and optimization. The significance of wave drag for high-speed aircraft plays major role on supersonic flow regime. Despite the fact that many other drag types play role on the calculation of the overall drag, wave drag coefficient describes the performance of aircraft at high speeds. Secondly, the solver is verified by using two different aircrafts the wave drag coefficients of which are obtained from

literature. It is seen that the difference between the results of the actual study and the literature results are in sufficiently close agreement so as to implement the optimization algorithm. Results are obtained from computational fluid dynamics simulations with a variety of supersonic flow speeds. $F-16$ aircraft is analyzed and obtained that error is smaller than 8%. Next, test cases are created with respect to the aerodynamic parameters. The case matrix is generated to analyze the effect of each aerodynamic parameter such as dihedral angle and area of the control surfaces. It is verified that various types of aircrafts could be optimized by using the algorithm. Although the optimal shape of each configuration has the smallest wave drag coefficient for the given volume and length, the manufacturability of these aircraft remains vague. In addition, geometry of the aircraft on use is optimized by employing the constraints related to the engine size in order to show the algorithm can be used not only theoretical but also practical approaches. Finally, the program has the ability to optimize the entire configuration. However, parts having no effect on the aerodynamic characteristics are enforced to body shape change. A main reason behind this is preventing from additional aerodynamic trade-off analysis while generating the final configuration of the designed aircraft. In conclusion, aircrafts which are environmentally friendly by saving fuel, and provides high-level security with better performance can be obtained as a result of the study. As a future aim, additional objective functions could be added to the program. Maximization of lift will be complementary for the optimization problem of the complete aircraft post-design.

References

1. Ashley, H., Landahl, M.: Aerodynamics of Wings and Bodies. Dover Publications, New York (1965)
2. Cahn, M.S., Olstad, W.B.: A Numerical Method for Evaluating Wave Drag. National Advisory Committee for Aeronautics, Langley Field (1958)
3. Citak, C.: Wave Drag Optimization of High Speed Aircraft. Middle East Technical University, Ankara (2015)
4. Citak, C., Ozgen, S.: Sesustu Hava Araclarinin Dalga Surukleme Katsayilarinin Sayisal Yontemlerle Hesaplanmasi, SAVTEK 2014, Ankara (2014)
5. Eminton, E.: On the Numerical Evaluation of the Drag Integral. Ministry of Aviation, London (1961)
6. Entsminger, A., David, G., Will G.: General Dynamics F-16 Fighting Falcon (2014)
7. Geiselhart, K.: Integration of Multifidelity Multidisciplinary Computer Codes for Design and Analysis of Supersonic Aircraft. AIAA
8. Griva, I., Nash, S.G., Sofer, A.: Linear and Nonlinear Optimization. Society for Industrial and Applied Mathematics, Philadelphia (2008)
9. Hepperle, M.: The Sonic Cruiser - A Concept Analysis, International Symposium "Aviation Technologies of the XXI Century: New Aircraft Concepts and Flight Simulation", Berlin, (2002)
10. Hutchison, M.G.: Multidisciplinary Optimization of High - Speed Civil Transport Configurations Using Variable - Complexity Modeling. Virginia Polytechnic Institute and State University, Blacksburg (1993)
11. Knill, O.: Multivariable Calculus - Lecture 21: Greens theorem. Harvard University, (2011)

12. Kribler, T.: A Conceptual Design Methodology to Predict the Wave Drag of a Transonic Wing, Aerodynamic Design and Optimization of Flight Vehicles in a Concurrent Multi-Disciplinary Environment, Ottawa (1999)
13. Rallabhandi, S.K., Mavris, D.N.: An Unstructured Wave Drag Code for Preliminary Design of Future Supersonic Aircraft. AIAA, Orlando (2003)
14. Raymer, Daniel P.: Aircraft Design: A Conceptual Approach. AIAA Education Series. Wiley, Reston (2012)
15. Roy Jr., V.: Harris, : An Analysis and Correlation of Aircraft Wave Drag. NASA Technical Memorandum. Langley Station, Hampton (1964)
16. Strang, W.J., McKinlay, R.: Concorde in Service. Aeronaut. J. **83**(818), 39–52 (1979)
17. Ward, G.N.: Linearized Theory of Steady High - Speed Flow. Cambridge University Press, Cambridge (1955)
18. Wikipedia (2014) Wikipedia GE F414
19. Wilhite, A.W.: An Overview of NASA's High - Speed Research Program, ICAS (2000)